Nanoscale

Accepted Manuscript

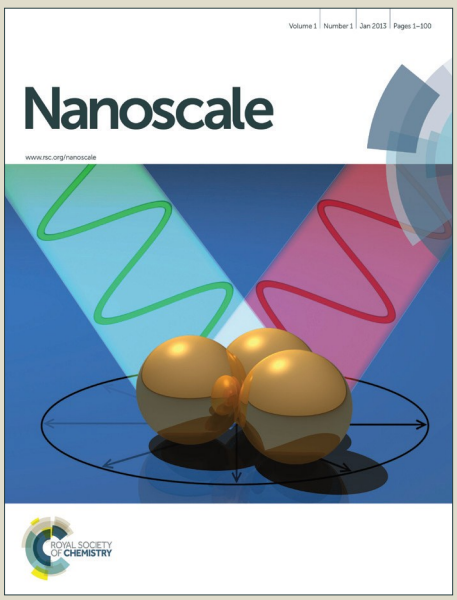

ROYAL SOCIETY OF CHEMISTRY

www.rsc.org/nanoscale

Cite this: DOI: 10.1039/c0xx00000x

www.rsc.org/xxxxxx

Paper

Label-free detection of DNA using light-addressable potentiometric sensor modified with a positively charged polyelectrolyte layer

Chunsheng Wu,[a,b] Thomas Bronder,[a] Arshak Poghossian,[a,c*] Carl Frederik Werner[a] and Michael J. Schöning[a,c]

Received (in XXX, XXX) Xth XXXXXXXXX 20XX, Accepted Xth XXXXXXXXX 20XX
DOI: 10.1039/b000000x

A multi-spot (16 spots) light-addressable potentiometric sensor (MLAPS) consisting of an Al–p-Si–SiO_2 structure modified with a weak polyelectrolyte layer of PAH (poly(allylamine hydrochloride) was applied for the label-free electrical detection of DNA (deoxyribonucleic acid) immobilization and hybridization by the intrinsic molecular charge for the first time. To achieve a preferentially flat orientation of DNA strands and thus, to reduce the distance between the DNA charge and MLAPS surface, the negatively charged probe single-stranded DNAs (ssDNA) were electrostatically adsorbed onto the positively charged PAH layer using a simple layer-by-layer (LbL) technique. In this way, more DNA charge can be positioned within the Debye length, yielding a higher sensor signal. The surface potential changes in each spot induced due to the surface modification steps (PAH adsorption, probe ssDNA immobilization, hybridization with complementary target DNA (cDNA), non-specific adsorption of mismatched ssDNA) were determined from the shifts of photocurrent-voltage curves along the voltage axis. A high sensor signal of 83 mV was registered after immobilization of probe ssDNA onto the PAH layer. The hybridization signal increases from 5 mV to 32 mV with increasing the concentration of cDNA from 0.1 nM to 5 µM. In contrast, a small signal of 5 mV was recorded in case of non-specific adsorption of fully mismatched ssDNA (5 µM). The obtained results demonstrate the potential of the MLAPS in combination with the simple and rapid LbL immobilization technique as a promising platform for a future development of multi-spot light-addressable label-free DNA chips with direct electrical readout.

Introduction

In recent years, deoxyribonucleic acid (DNA) biosensors have been increasingly recognized as an emerging and promising technique in many fields of application, including DNA diagnostic, gene analysis, parental testing, forensic science and drug industry.[1–3] Most of the DNA-detection techniques are based on a specific DNA-hybridization event between an immobilized probe single-stranded DNA (ssDNA) and a complementary target DNA (cDNA). Various transducer principles such as piezoelectric, optical, and electrochemical have been used to detect the DNA-hybridization event.[1,4,5] However, DNA biosensors often require labeling of either the probe or target DNA using various markers (e.g., redox, enzymatic, radiochemical, chemiluminescence or fluorescence).[1–7] Although the labeling procedure provides a high sensitivity, it has been proven to be complicated, time-consuming and expensive.[1,7,8] In this context, DNA-hybridization detection techniques based on label-free principles are preferred, because they would significantly reduce the cost and time needed for sample preparation and modification of the target molecules.[9,10]

Among various device concepts proposed for the label-free detection of DNA hybridization (e.g., quartz crystal microbalance,[11] surface plasmon resonance,[11,12] fluorescence resonance energy transfer,[13,14] faradaic and non-faradaic impedimetry,[15-18] the semiconductor field-effect device (FED) platform, which is based on an electrostatic detection of the intrinsic negative charge of DNA molecules with direct electrical readout, is one of the most attractive approaches.[2,10] FEDs based on an electrolyte-insulator-semiconductor (EIS) system, like ion-sensitive field-effect transistors (ISFET), capacitive EIS sensors, light-addressable potentiometric sensors (LAPS) and silicon nanowires (SiNW), are known as surface-charge sensitive devices and have been widely applied for the detection of various analytes in liquids as well as charged molecules or charged nanoparticles.[2,10,19–32] However, because of screening of the intrinsic charge of molecules by small ions in the surrounding solution, FEDs are able to detect the charge changes that occur directly at the gate surface or within the order of the Debye screening length (the Debye length is inversely proportional to the ionic strength of the solution; it amounts, for instance, ~0.3 nm in 1 M electrolyte solution containing monovalent ions and ~0.8 nm in physiologically relevant solutions with an ionic strength of ~150 mM) from the surface only.[2,28,33,34] As a consequence, the electrostatic coupling between the charged molecule and the FED strongly depends on the ionic strength of the solution and the distance between the charge of the molecule and the gate surface. Moreover, if the molecular charge is distributed along the molecule length (as for instance, in the case of DNA molecules), the FED signal will also depend on an orientation of molecules to the gate surface.[35–37] Thus, in addition to the charge-screening effect, the surface functionalization and DNA-immobilization technique has strong impact on the DNA-

hybridization signal. For example, if the DNA molecules are tethered to the gate surface via linker molecules or spacer, the DNA-hybridization induced FED signal will strongly drop with increasing the length of linker molecules. To reduce the charge-screening effect and thus, to enhance the sensitivity of the FEDs to the molecular charge, experiments on detection of charged molecules with FEDs are often performed in low ionic-strength solutions (see e.g., ref. 38). The price to be paid is a reduced probability of hybridization and therefore, an extended hybridization time (due to the electrostatic repulsion between the complementary DNA strands).

The most experiments on a field-effect detection of DNA have been carried out using different types of ISFETs, capacitive EIS sensors or SiNWs.[2,25,28,39] At the same time, in spite of popularity of LAPS in many chemical and biological applications (e.g., measurement of pH and ion concentration, enzymatic reactions, acidification rate of living cells),[40–42] it is very little known about LAPS-based DNA biosensors. Only recently, LAPS with a TiO_2 gate and multi-spot LAPS (MLAPS) with a SiO_2 gate have been applied for the label-free electrical detection of DNA immobilization and hybridization.[43,44] In both works, probe ssDNA molecules were covalently immobilized onto the gate surface that requires time-consuming, cost-expensive procedures and complicated chemistry for functionalization of the gate surface and/or probe ssDNA. Therefore, an exploration of novel approaches to optimize and simplify the immobilization process of probe ssDNA is highly important for a new generation of label-free DNA chips based on LAPS devices. In this context, non-covalent surface attachment of probe ssDNA using electrostatic and/or hydrophobic interactions becomes more and more popular in DNA sensor design, including FED-based DNA biosensors.[38,45–47]

In this work, we present a new MLAPS-based DNA biosensor, where a simple strategy is used for a rapid immobilization of probe ssDNA molecules onto the gate surface via the layer-by-layer (LbL) electrostatic adsorption of a weak-polyelectrolyte/ssDNA bilayer, and the subsequent label-free detection of DNA hybridization. If probe ssDNA molecules preferentially lie flat for the full length on the LAPS surface with negatively charged phosphate groups directed to the positively charged polyelectrolyte layer (in this study, poly(allylamine hydrochloride) (PAH)) and the bases are exposed to the surrounding solution and ready for the hybridization with complementary target DNA molecules, both the Debye screening effect and the electrostatic repulsion between target and probe DNA molecules are less effective, and therefore, a higher hybridization signal can be expected.

DNA immobilization and hybridization

In order to reduce the distance between the DNA charge and sensor surface, the probe ssDNAs were physically adsorbed onto the PAH-modified MLAPS surface by electrostatic interaction. Because a SiO_2 surface is negatively charged at a physiological pH, it is necessary to coat the surface with a positively charged layer for an electrostatic adsorption of probe ssDNA.

The LbL-assembly technique was used for both the adsorption of positively charged PAH macromolecules on the negatively charged SiO_2 layer and the immobilization of negatively charged probe ssDNA molecules on a positively charged PAH layer. The LbL technique provides a simple, fast, low-cost and efficient method for the preparation of ultrathin films as well as complex heterostructures with a well-defined composition and functionality, whereby ultrathin films are assembled electrostatically from the repetitive, sequential adsorption of polyions with alternating charge.[27,45,48,49]

As it has been discussed in ref. 45, the LbL immobilization of ssDNA usually results in a formation of flat elongated structures, a crucial factor to enhance the sensitivity of the MLAPS to the DNA charge. Although, the electrostatic adsorption of the probe ssDNA may not provide the strong binding to the sensor surface, the advantage of adsorptive immobilization is that the ssDNAs lay down on the surface instead of standing up. In that way, more negative charge of the probe ssDNA molecules can be positioned near the gate surface within the Debye length. In addition, the positively charged PAH layer may reduce the electrostatic repulsion between probe and complementary target ssDNA molecules and thus, may accelerate the hybridization process. It can be expected that after hybridization, the dsDNA molecules will also lay flat on the MLAPS surface. Thus, the full dsDNA charge could probably be within the Debye length yielding a higher sensor signal.

The PAH layer was deposited onto the SiO_2 surface from the PAH solution (10 µM, 50 µM or 100 µM PAH adjusted with 10 mM NaCl, pH 5.4) in accordance to the procedure described in ref. 27. At pH 5.4, the weak polyelectrolyte PAH is fully charged.[50] On the other hand, in the solution of pH 5.4, the surface of SiO_2 can be considered enough negatively charged (the pHpzc at point of zero charge of SiO_2 is about 2.5) to provide electrostatic adsorption of PAH molecules.[51] During the experiments, the cleaned SiO_2 surface of the MLAPS chip was exposed to PAH solution for about 10 min at room temperature, followed by a rinsing step and exposing to the probe ssDNA immobilization solution (5 µM ssDNA dissolved in 1× TE buffer (10 mM Tris (tris(hydroxymethyl)aminomethane), 1 mM EDTA (ethylenediaminetetraacetic acid), pH 8) for 30 min. Finally, the MLAPS surface was washed with measurement solution (10 mM NaCl, pH 5.4) for 3 times to remove non-attached molecules from the sensor surface. For hybridization of probe ssDNA with complementary target ssDNA, the MLAPS surface was exposed to the hybridization solution (5 µM target ssDNA, 10 mM Tris, 1 mM EDTA, pH 8) for 30 min at room temperature, followed by washing for 3 times with measurement solution to remove the non-hybridized target DNA molecules and finally, drying with nitrogen stream. To study the detection limit of the developed MLAPS-based DNA biosensor as well as an impact of mismatched ssDNAs on the MLAPS signal, the sensor surface was exposed to hybridization solution containing different concentrations of cDNA (from 0.1 nM to 5 µM) or 5 µM mismatched ssDNA, respectively, using the same protocol above. The hybridization solutions with different concentrations of cDNA were prepared from 5 µM cDNA solution by dilution in TE buffer.

Functioning of the MLAPS

The MLAPS has been applied for the label-free detection of DNA hybridization for the first time in ref. 44. Fig. 1 shows a schematic structure and measurement setup of the MLAPS for DNA immobilization and hybridization detection. The capacitance of the depletion layer in the semiconductor depends on the applied bias voltage and the potential or charge changes at the gate insulator/electrolyte interface. In order to detect the variations of the depletion capacitance, the LAPS is illuminated with a modulated light, which induces an alternating photocurrent to be measured as the sensor signal.[52,53] Since PAH molecules are positively charged and DNA molecules are polyanions, it can be expected that PAH adsorption, probe ssDNA immobilization, and target cDNA hybridization occurred on the gate surface of the MLAPS will effectively alter the charge applied to the gate. This

will lead to a modulation of the flat-band potential and consequently, the photocurrent of the LAPS. The signal from each spot on the LAPS gate surface can be read out by focusing a modulated irradiation there. Moreover, by using an array of light-emitting diodes (LED), where all LEDs illuminate simultaneously, the LAPS is able for parallel multi-spot measurements (MLAPS setup).[54] This feature makes MLAPS as a very attractive transducer platform for high-throughput parallel measurements of multiple analytes, in particular, for the development of light-addressable DNA chips.

In this study, an array consisting of 4 × 4 infrared LEDs with a wavelength of 950 nm was utilized as light source for the photocurrent generation. In the MLAPS setup, 16 spots on the rear-side Si surface are illuminated in parallel by using 16 LEDs with different modulation frequencies. A field-programmable gate array (FPGA) was used to control the modulation frequency of each LED.[54] To reduce the influence of the charge-screening effect, all measurements were performed in the same low ionic-strength solution (10 mM NaCl, pH 5.4). For the measurement of the photocurrent-voltage (*I-V*) curve, a bias voltage ranging from –0.8 V to +0.8 V is applied between a conventional liquid-junction Ag/AgCl reference electrode (Metrohm, 3 M KCl) and the rear-side Al contact. The *I-V* curves of all 16 measurement spots were simultaneously recorded every 10 s. The local surface-potential changes in each measurement spot induced due to the surface modification steps (e.g., PAH adsorption, probe ssDNA immobilization, target cDNA hybridization) were determined from the shifts of *I-V* curves along the voltage axis.

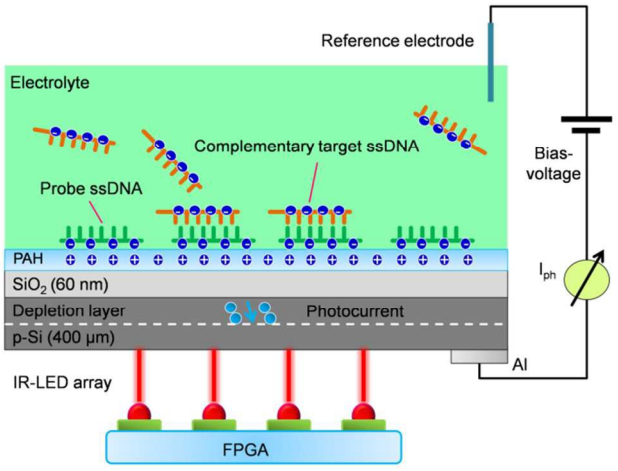

Fig. 1 Schematic layer structure and measuring setup of the MLAPS-based DNA biosensor. FPGA: field-programmable gate array; I_{ph}: measured photocurrent.

For a correct functioning of the MLAPS, leakage current between the reference electrode and rear-side contact should be very small. Therefore, only chips having leakage current less than 20 nA were utilized for further DNA detection experiments. In addition, the sensitivity of the MLAPS chips to surface-charge changes have been tested by means of a measurement of shifts of *I-V* curves in various pH buffer solutions from pH 3 to pH 9. According to the site-binding model,[55] the surface charge of oxides (in this work, SiO_2) is affected by the pH value of solution. The mean pH sensitivity evaluated from the shifts in the depletion range of the *I-V* curves for 16 spots was 43 mV/pH, which is comparable to values previously reported for thermally grown SiO_2 layers (see e.g., ref. 28, 56). These results demonstrate the suitability of the developed MLAPS devices as charge-sensitive transducer for further experiments on label-free detection of DNA molecules by their intrinsic molecular charge.

Results and discussion

Electrical detection of PAH adsorption and probe ssDNA immobilization

To investigate the effect of the PAH concentration on the adsorption of the PAH layer and subsequent electrostatic immobilization of probe ssDNA molecules, PAH layers were prepared from solutions of 10 µM, 50 µM and 100 µM PAH adjusted with 10 mM NaCl. The pH value of all PAH solutions was adjusted to pH 5.4. Fig. 2 depicts potential shifts (averaged over 16 measurement spots) evaluated from the inflection points of *I-V* curves of bare MLAPS, and after consecutive LbL adsorption of PAH and probe ssDNA (5 µM) molecules.

The consecutive adsorption of oppositely charged PAH and DNA layers leads to alternating potential shifts (MLAPS signal) for about 30 and 82 mV, respectively. The direction of these potential shifts depends on the sign of the charge of the adsorbed outermost layer, while the amplitude reflects the amount of adsorbed charge. Qualitatively, the signal behaviour of the MLAPS can be explained as follows: if a positively charged PAH layer is adsorbed onto the negatively charged SiO_2 surface, one needs to apply a more negative gate voltage to compensate for this positive charge and to keep the photocurrent constant. In contrast, the adsorption of negatively charged probe ssDNA molecules shifts the sensor signal towards the direction of more positive (or less negative) bias voltages.

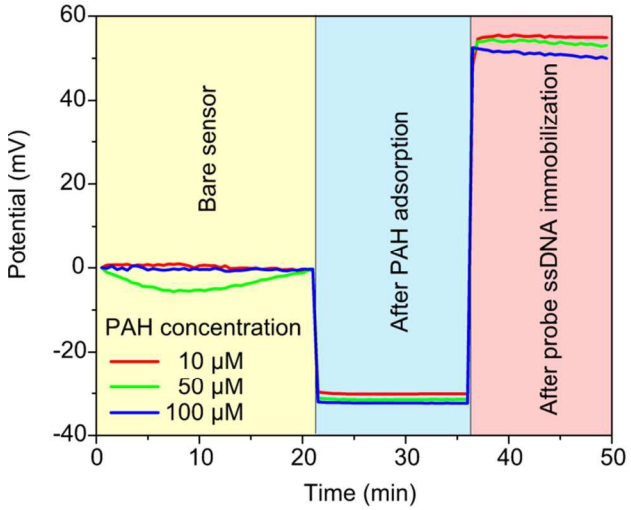

Fig. 2 Potential shifts (MLAPS signal) evaluated from the inflection points of *I-V* curves of bare MLAPS and after consecutive LbL adsorption of PAH and probe ssDNA (5 µM) molecules. The PAH layer was prepared from the solutions with different PAH concentrations of 10 µM, 50 µM and 100 µM. The measured data were averaged over 16 measurement spots.

As can be seen from Fig. 2, the PAH concentration in polyelectrolyte solution does not significantly affect the amplitude of potential shifts (at least in the range of PAH concentrations used in this study). This can be explained by suggesting a nearly identical amount of adsorbed PAH molecules on the SiO_2 gate surface for all three PAH concentrations used in

this experiment. In addition, likely, nearly the same amount of probe ssDNA was immobilized on the MLAPS surface modified with PAH layers prepared from the PAH solutions of different concentrations. Therefore, in further experiments the PAH layer was prepared from 10 μM PAH solution. These results clearly demonstrate that reproducible PAH/DNA bilayers on the MLAPS surface can be formed via simple, cost-effective and fast LbL adsorption technique.

To investigate the effect of the probe ssDNA concentration on the immobilization signal, the probe molecules were immobilized from solutions of 0.5 μM, 2.5 μM, 5 μM, 7.5 μM and 10 μM ssDNA. These results are presented in the electronic supplementary information available on the website. With increasing ssDNA concentration from 0.5 μM to 5 μM, the immobilization signal increases from 55 mV to 80 mV. Further increase of the ssDNA concentration results in a less stable immobilization signal. As a consequence, in further experiments, probe molecules were immobilized from a 5 μM ssDNA solution.

Label-free detection of DNA hybridization

During hybridization experiments, the *I-V* curves of MLAPS were recorded simultaneously in 16 spots before and after each surface functionalization step using the same low ionic-strength measurement solution (10 mM NaCl, pH 5.4). Fig. 3 shows typical normalized *I-V* curves (a) and zoomed *I-V* curves in depletion region (b) recorded from the single spot (spot 10) before and after PAH adsorption, after probe ssDNA immobilization, after non-specific adsorption of fully mismatched ssDNA molecules, and after hybridization of probe ssDNAs with complementary targed cDNAs. As expected, adsorption of positively charged PAH shifts the original *I-V* curve of the bare MLAPS towards the direction of more negative (or less positive) bias voltages, while the adsorptive immobilization of negatively charged probe ssDNAs and subsequent hybridization with complementary target cDNAs (5 μM) results in a shift of the *I-V* curves towards the direction of more positive (or less negative) bias voltages. The DNA immobilization and hybridization signals evaluated from the *I-V* curves recorded from the spot 10 were 81 mV and 30 mV, respectively.

Fig. 4 depicts a dynamic mean response of the MLAPS before and after PAH adsorption, after probe ssDNA immobilization, after non-specific adsorption of fully mismatched ssDNA molecules, and after hybridization of probe ssDNAs with complementary targed cDNAs (5 μM). In this experiment, the mean potential shifts (averaged over 16 measurement spots) were evaluated from the inflection points of the respective *I-V* curves. The *I-V* curves from all 16 spots were collected simultaneously every 10 s. The mean immobilization and hybridization signals were 83 mV and 32 mV, respectively. At the same time, non-specific adsorption of fully mismatched ssDNAs induces only a small potential shift of less than 5 mV. The hybridization signals detected by the MLAPS functionalized with a PAH/DNA LbL layer were about 5 times higher than that of the capacitive EIS sensor[38] or floating-gate transistor structure[47] modified with poly-L-lysine/DNA LbL layer and comparable with hybridization signals recorded by the MLAPS,[44] capacitive EIS sensors[57] and silicon nanowires[58] with probe ssDNAs covalently attached to the silanized SiO_2 gate surface. In general, the hybridization signal was smaller than the immobilization signal. This is in consistence with the results reported previously (see e.g., ref. 33, 58).

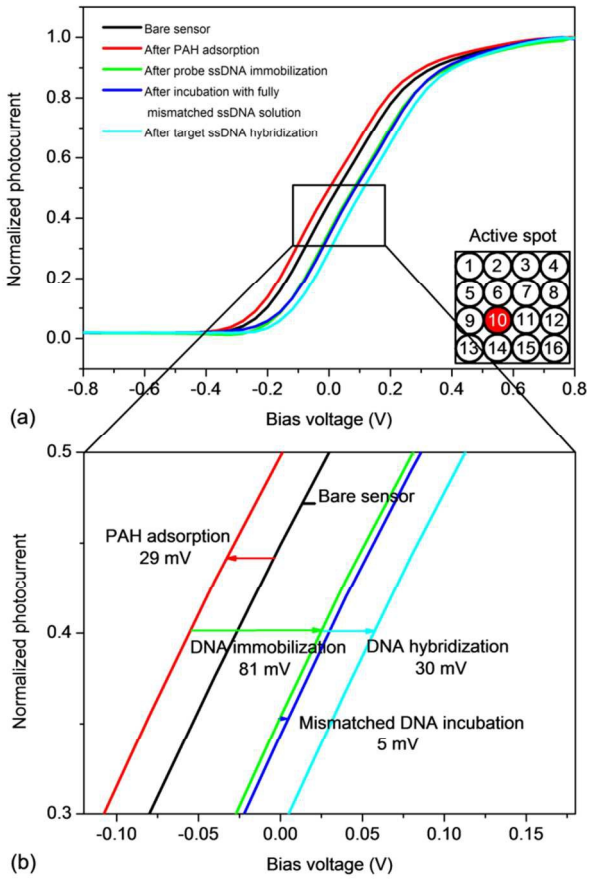

Fig. 3 Typical normalized I-V curves (a) and zoomed I-V curves in depletion region (b) recorded from the single spot (spot 10) before and after PAH adsorption, after probe ssDNA immobilization, after non-specific adsorption of fully mismatched ssDNA molecules, and after hybridization of probe ssDNAs with complementary target cDNAs. The normalized photocurrent represents the ratio of an actual photocurrent to the maximum photocurrent in the inversion region.

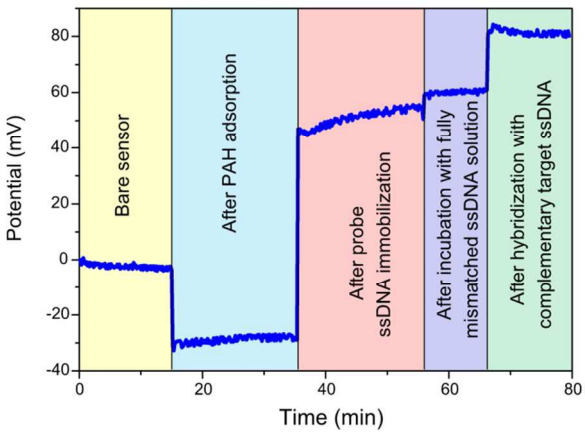

Fig. 4 Dynamic mean response of the MLAPS before and after PAH adsorption, after probe ssDNA immobilization, after non-specific adsorption of fully mismatched ssDNA molecules, and after hybridization of probe ssDNAs with complementary target cDNAs. The measured data were averaged over 16 measurement spots.

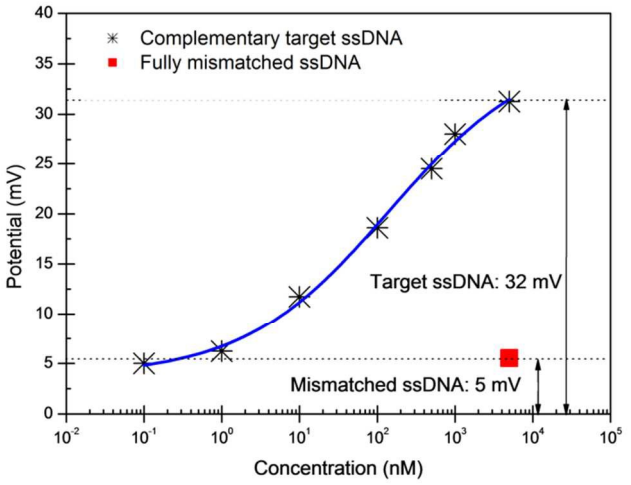

Fig. 5 Dependence of the hybridization signal of the MLAPS (averaged over 16 spots) on target cDNA concentration ranging from 0.1 nM to 5 µM. For comparison, the response of the sensor to 5 µM fully mismatched ssDNA is presented, too.

Fig. 5 presents the dependence of the hybridization signal of the MLAPS (averaged over 16 spots) on target cDNA concentration ranging from 0.1 nM to 5 µM. To demonstrate the specificity of the MLAPS, the response of the sensor to 5 µM fully mismatched ssDNA is presented, too. The hybridization signal increases with increasing the target cDNA concentration and achieves a value of 32 mV at 5 µM cDNA. Even at a very low cDNA concentration of 0.1 nM, a detectable hybridization signal of 5 mV has been registered. The observed potential shift of about 5 mV due to non-specific adsorption of fully mismatched ssDNA was similar to that observed after hybridization of cDNA with a more than four orders of magnitude smaller concentration of 0.1 nM (see Fig. 5). These studies indicate a good specificity of the developed MLAPS capable for distinguishing a complementary sequence from mismatched sequences even at very low concentrations of cDNA (in nM range).

Conclusions

Due to their small sizes and compatibility with advanced micro- and nanofabrication technologies, semiconductor field-effect devices offer new opportunities for label-free DNA chips with direct electronic readout for fast, simple, and inexpensive real-time analysis of nucleic acid samples. In this work, the field-effect MLAPS consisting of an Al-p-Si-SiO_2 structure modified with a weak polyelectrolyte PAH layer has successfully been applied for the label-free electrical detection of DNA immobilization and hybridization by the intrinsic molecular charge for the first time. The simple LbL technique was used for both the electrostatic adsorption of positively charged PAH macromolecules on the negatively charged SiO_2 layer and rapid immobilization of negatively charged probe ssDNA molecules on the positively charged PAH layer. The advantage of the adsorptive immobilization is that the probe ssDNAs as well as dsDNAs (after hybridization) preferentially lay flat on the MLAPS surface. In that way, more dsDNA charge can be positioned near to the gate surface within the Debye length, yielding a higher sensor signal.

In the MLAPS setup, 16 spots on the rear-side Si surface were illuminated in parallel by using 16 LEDs with different modulation frequencies and the *I-V* curves were simultaneously recorded on all spots. The local surface-potential changes in each measurement spot induced due to the surface modification steps (i.e., PAH adsorption, probe ssDNA immobilization, non-specific adsorption of mismatched ssDNA, hybridization with cDNA) were determined from the shifts of *I-V* curves along the voltage axis. The large immobilization signal of 83 mV (averaged over 16 spots) has been observed after LbL immobilization of probe ssDNA onto the positively charged PAH layer. The MLAPS hybridization signal shows a distinct dependence on the concentration of cDNA. The hybridization signal increases from 5 mV to 32 mV with increasing the concentration of cDNA from 0.1 nM to 5 µM. At the same time, a small potential shift of ~5 mV was recorded in case of non-specific adsorption of fully mismatched ssDNA with a concentration of 5 µM. This confirms that our device is able to differentiate between complementary and mismatched DNA sequences. Nevertheless, the detection limit is still far from those reported for labeling methods.

The obtained results demonstrate the potential of the MLAPS as promising transducer platform for multi-spot label-free electrical detection of DNA molecules by their intrinsic molecular charge. Future work will be directed to enhance the detection limit, to develop a light-addressable multi-spot DNA chip by immobilizing each spot of MLAPS with various ssDNA sequences as well as to realize differential-mode measurements between spots, including the detection of single-nucleotide polymorphisms.

Experimental methods

Fabrication of MLAPS chips

MLAPS chips consisting of an Al-Si-SiO_2 structure were fabricated using a p-doped silicon wafer (<100>, resistivity 1–10 Ωcm, 400 µm in thickness) and standard microfabrication processes. A 60 nm thick SiO_2 gate-insulator layer was prepared by thermal dry oxidation of Si at 1050 °C for about 45 min. Then, the SiO_2 layer on the rear side of the silicon wafer was etched and a 300 nm thick Al layer was deposited as an Ohmic contact to Si. After fabrication, the wafer was cut into separate chips with sizes of 2.0 cm × 2.0 cm. Finally, on the rear side of the MLAPS chip, the Al layer was structured by etching to open a window for the backside illumination of Si.

MLAPS setup

By simultaneous illumination of multiple spots, the measured photocurrent is a superposition of local photocurrents modulated with different frequencies, i.e. contains information from all measurement spots. Photocurrent changes from individual measurement spots induced by the adsorption or binding of charged molecules on the gate surface can be separated and determined from the overall photocurrent by means of a fast Fourier transformation (FFT) algorithm. The shifts of *I-V* curves are calculated automatically and can be presented in the form of a time-dependent potential shift for each individual spot or average shift for all 16 spots. The diameter of the spot illuminated by the single LED was about 2 mm. The modulation frequencies of LEDs range from 1 kHz to 1.75 kHz with the frequency step width of 50 Hz. The measurement data were collected by a data-acquisition card (DAQmx PCI-6259, National Instruments, USA). The whole MLAPS measurement system was controlled by a customized LabVIEW software.

For the experiments, the MLAPS chip was mounted into a home-made detection chamber and connected to the measurement system for photocurrent studies. The effective contact area of the

MLAPS front surface with the solution was about 1.4 cm × 1.4 cm. The pH value of all solutions was controlled with a Mettler-Toledo MPC227 pH/Conductivity Meter. The measurements were carried out at room temperature. The measurement setup was shielded with a Faraday box to reduce the influence of ambient light and electromagnetic fields. All potential values are referred to the reference electrode

DNA sequences

The sequences of 20 mer probe, target and mismatched ssDNA molecules used in this study were purchased from Biomers (Biomers GmbH, Ulm, Germany) and are presented in Table 1.

Table 1. The sequences of probe, target and mismatched ssDNA molecules used in this study.

Type	Sequence
probe ssDNA	5'-ACCTGGGGGAGTATTGCGGA-3'
complementary target cDNA	5'-TCCGCAATACTCCCCCAGGT-3'
fully mismatched ssDNA	5'-AGGCGTTATGAGGGGGTCCA-3'

Acknowledgements

This work was partially supported by the Bundesministerium für Bildung und Forschung (BMBF) (DiaCharge project), the National Natural Science Foundation of China (Grant No. 31470956), and the Zhejiang Provincial Natural Science Foundation of China (LY13H180002).

References

1 A. Sassolas, B. D. Leca-Bouvier and L. J. Blum, *Chem. Rev.*, 2008, **108**, 109–139.

2 A. Poghossian and M. J. Schöning, *Electroanal.*, 2014, **26**, 1197–1213.

3 S. Choi, M. Goryll, L. Y. M. Sin, P. K. Wong and J. Chae, *Microfluid. Nanofluidics*, 2010, **10**, 231–247.

4 E. Palecek and M. Bartosik, *Chem. Rev.*, 2012, **112**, 3427–3481.

5 A. Liu, K. Wang, S. Weng, Y. Lei, L. Lin, W. Chen, X. Lin and Y. Chen, *Trends Anal. Chem.*, 2012, **37**, 101–111.

6 H. Chen, C. Jiang, C. Yu, S. Zhang, B. Liu and J. Kong, *Biosens. Bioelectron.*, 2009, **24**, 3399–3411.

7 M. Javanmard and R. W. Davis, *Sens. Actuators B*, 2011, **154**, 22–27.

8 C. Batchelor-McAuley, G. G. Wildgoose and R. G. Compton, *Biosens. Bioelectron.*, 2009, **24**, 3183–3190.

9 S. Mehrabani, A. J. Maker and A. M. Armani, *Sensors*, 2014, **14**, 5890–5928.

10 C.-C. Wu, F.-H. Ko, Y.-S. Yang, D.-L. Hsia, B.-S. Lee and T.-S. Su, *Biosens. Bioelectron.*, 2009, **25**, 820–825.

11 S. Cagnin, M. Caraballo, C. Guiducci, P. Martini, M. Ross, M. Santaana, D. Danley, T. West and G. Lanfranchi, *Sensors*, 2009, **9**, 3122–3148.

12 B. P. Nelson, T. E. Grimsrud, M. R. Liles, R. M. Goodman and R. M. Corn, *Anal. Chem.*, 2001, **73**, 1–7.

13 C. Xu, R. Zhou, R. Zhang, L. Yang and G. Wang, *ACS Macro Lett.*, 2014, **3**, 845-848.

14 R. Zhou, C. Xu, J. Dong and G. Wang, *Biosens. Bioelectron.*, 2015, **65**, 103-107.

15 M. Lazerges and F. Bedioui, *Anal. Bioanal. Chem.*, 2013, **405**, 3705–3714.

16 J. S. Daniels and N. Pourmand, *Electroanal.*, 2007, **19**, 1239–1257.

17 J.-Y. Park and S.-M. Park, *Sensors*, 2009, **9**, 9513–9532.

18 M. Riedel, J. Kartchemnik, M. J. Schöning and F. Lisdat, *Anal. Chem.*, 2014, **86**, 7867–7874.

19 A. Poghossian, *Sens. Actuators B*, 1992, **7**, 367–370.

20 M. J. Schöning, N. Näther, V. Auger, A. Poghossian and M. Koudelka-Hep, *Sens. Actuators B*, 2005, **108**, 986–992.

21 A. Poghossian, D.-T. Mai, Y. Mourzina and M. J. Schöning, *Sens. Actuators B*, 2004, **103**, 423–428.

22 C. Jimenez-Jorquera, J. Orozco and A. Baldi, *Sensors*, 2010, **10**, 61–83.

23 C.-S. Lee, S. K. Kim and M. Kim, *Sensors*, 2009, **9**, 7111–7131.

24 K. Nakazato, *Sensors*, 2009, **9**, 8831–8851.

25 E. Stern, A. Vacic and M. A. Reed, *IEEE T. Electron. Dev.*, 2008, **55**, 3119–3130.

26 N. Lu, A. Gao, P. Dai, T. Li, Y. Wang, X. Gao, S. Song, C. Fan and Y. Wang, *Methods*, 2013, **63**, 212–218.

27 A. Poghossian, M. Weil, A. G. Cherstvy and M. J. Schöning, *Anal. Bioanal. Chem.*, 2013, **405**, 6425–6436.

28 M. H. Abouzar, A. Poghossian, A. G. Cherstvy, A. M. Pedraza, S. Ingebrandt and M. J. Schöning, *Phys. Status Solidi A*, 2012, **209**, 925–934.

29 A. Kulkarni, Y. Xu, C. Ahn, R. Amin, S. H. Park, T. Kim and M. Lee, *J. Biotechnol.*, 2012, **160**, 91–96.

30 J. Gun, M. J. Schöning, M. H. Abouzar, A. Poghossian and E. Katz, *Electroanal.*, 2008, **20**, 1748–1753.

31 A. Poghossian, M. Thust, P. Schroth, A. Steffen, H. Lüth and M.J. Schöning, *Sens. Mater.*, 2001, **13**, 207–223.

32 A. Poghossian, M. Bäcker, D. Mayer and M.J. Schöning, *Nanoscale*, 2014, DOI:10.1039/c4nr05987e.

33 Y. Liu and R. W. Dutton, *J. Appl. Phys.*, 2009, **106**, 014701.

34 G.-J. Zhang, G. Zhang, J. H. Chua, R.-E. Chee, E. H. Wong, A. Agarwal, K. D. Buddharaju, N. Singh, Z. Gao and N. Balasubramanian, *Nano Lett.*, 2008, **8**, 1066–1070.

35 Y. Nishio, S. Uno and K. Nakazato, *Jpn. J. Appl. Phys.*, 2013, **52**, 04CL01.

36 U. Rant, K. Arinaga, S. Fujita, N. Yokoyama, G. Abstreiter and M. Tornow, *Org. Biomol. Chem.*, 2006, **4**, 3448–3455.

37 S. Uno, M. Iio, H. Ozawa and K. Nakazato, *Jpn. J. Appl. Phys.*, 2010, **49**, 1–8.

38 J. Fritz, E. B. Cooper, S. Gaudet, P. K. Sorger and S. R. Manalis, *Proc. Natl. Acad. Sci. U. S. A.*, 2002, **99**, 14142–14126.

39 C. Kataoka-Hamai and Y. Miyahara, *IEEE Sens. J.*, 2011, **11**, 3153–3160.

40 J. C. Owicki, L. J. Bousse, D. G. Hafeman, G. L. Kirk, J. D. Olson, H. G. Wada and J. W. Parce, *Annu. Rev. Biophys. Biomol. Struct.*, 1994, **23**, 87–113.

41 J. R. Siqueira, R. M. Maki, F. V. Paulovich, C. F. Werner, A. Poghossian, M. C. F. De Oliveira, V. Zucolotto, O. N. Oliveira and M. J. Schöning, *Anal. Chem.*, 2010, **82**, 61–65.

42 B. Stein, M. George, H. E. Gaub and W. J. Parak, *Sens. Actuators B*, 2004, **98**, 299–304.
43 X. Zong, C. Wu, X. Wu, Y. Lu and P. Wang, *J. Zhejiang Univ. Sci. B*, 2009, **10**, 860–866.
44 C. Wu, T. Bronder, A. Poghossian, C. F. Werner, M. Bäcker and M. J. Schöning, *Phys. Status Solidi A*, 2014, **211**, 1423–1428.
45 G. A. Evtugyn and T. Hianik, *Curr. Anal. Chem.*, 2011, **7**, 8–34.
46 Y. L. Bunimovich, Y. S. Shin, W. Yeo, M. Amori, G. Kwong and J. R. Heath, *J. Am. Chem. Soc.*, 2006, **128**, 16323–16331.
47 D. Braeken, G. Reekmans, C. Zhou, B. van Meerbergen, G. Callewaert, G. Borghs and C. Bartic, *J. Exp. Nanosci.*, 2008, **3**, 157–169.
48 M. Schönhoff, V. Ball, A. R. Bausch, C. Dejugnat, N. Delorme, K. Glinel, R. V. Klitzing and R. Steitz, *Colloids Surf., A*, 2007, **303**, 14–29.
49 J. R. Siqueira, M. H. Abouzar, M. Bäcker, V. Zucolotto, A. Poghossian, O. N. Oliveira and M. J. Schöning, *Phys. Status Solidi A*, 2009, **206**, 462–467.
50 R. N. Smith, M. McCormick, C. J. Barrett, L. Reven and H. W. Spiess, *Macromolecules*, 2004, **37**, 4830–4838.
51 A. Poghossian, *Sens. Actuators B*, 1997, **44**, 361–364.
52 T. Yoshinobu, H. Ecken, A. Poghossian, A. Simonis, H. Iwasaki, H. Lüth and M.J. Schöning, M.J., *Electroanal.*, 2001,**13**, 733**–**736.
53 J.R. Siqueira, Jr., C.F. Werner, M. Bäcker, A. Poghossian, V. Zucolotto, O.N. Oliveira, Jr. and M.J. Schöning, *J. Phys. Chem. C*, 2009, **113**, 14765–14770.
54 C. F. Werner, S. Schusser, H. Spelthahn, T. Wagner, T. Yoshinobu and M. J. Schöning, *Electrochim. Acta*, 2011, **56**, 9656–9660.
55 P. Bergveld, *Sens. Actuators B*, 2003, **88**, 1–20.
56 C. Cane, I. Gracia and A. Merlos, *Microelec. J.*, 1997, **28**, 389–405.
57 A. Poghossian, M. H. Abouzar, F. Amberger, D. Mayer, Y. Han, S. Ingebrandt, A. Offenhäusser and M. J. Schöning, *Biosens. Bioelectron.*, 2007, **22**, 2100–2107.
58 S. Ingebrandt, X. T. Vu, J. F. Eschermann, R. Stockmann and A. Offenhäusser, *ECS Trans.*, 2011, **35**, 3–15.

Notes

[a]*Institute of Nano- and Biotechnologies, FH Aachen, Campus Jülich, 52428 Jülich, Germany*
[b]*Biosensor National Special Laboratory, Key Laboratory for Biomedical Engineering of Ministry of Education, Department of Biomedical Engineering, Zhejiang University, Hangzhou 310027, China*
[c]*Peter Grünberg Institute (PGI-8), Research Centre Jülich GmbH, 52425 Jülich, Germany*
[*]*Corresponding author: Arshak Poghossian (email: a.poghossian@fz-juelich.de)*